

# Beam-Target Helicity Asymmetry $E$ in $K^+\Sigma^-$ Photoproduction on the Neutron

Nicholas Zachariou\* and Daniel Watts  
*University of York*

Andrey Sarantsev and Victor Nikonov  
*Bonn University*

(The CLAS Collaboration)  
(Dated: December 4, 2019)

We report a measurement of a beam-target double polarisation observable ( $E$ ) for the  $\vec{\gamma}\vec{n} \rightarrow K^+\Sigma^-$  reaction. The data were obtained using the circularly polarised energy-tagged photon beam of Hall B at Jefferson Lab with a spin-polarized solid hydrogen deuteride (HD) nuclear target. The  $E$  observable was determined for centre-of-mass energies  $1.70 \leq W \leq 2.30$  GeV, with reaction products detected over a wide angular acceptance by the CLAS spectrometer. This new double-polarisation data gives unique constraints on the strange decays of excited neutron states. Inclusion of the new data within the Bonn-Gatchina theoretical model results in significant changes for the extracted photocouplings of a number of established nucleon resonances. Compatibility of the new data with “missing” states including the  $D_{13}(2120)$  resonance are also explored.

## I. INTRODUCTION

A central aim of hadron spectroscopy is to obtain a deeper understanding of how bound quark systems form, starting from their fundamental partonic degrees of freedom (the quarks and gluons). Fundamental properties of bound quark systems provide an important challenge to quantum chromodynamics (QCD), and its ability to fully describe the non-perturbative phenomena underlying hadron structure [1]. Although the nucleon is probably the most abundant bound quark system in the universe, fundamental gaps remain in our knowledge of its dynamics and structure. Valuable information on the dynamics and properties of many-body systems are contained in their excitation spectra. Predictions of the nucleonic excitation spectra in QCD based approaches, e.g. phenomenological constituent quark models [2–7], lattice QCD [8–10] and string theory based AdS/QCD [11], predict many more excited states than currently established in experiment. Consequently, the “missing resonance” problem is an important focus for the world’s electromagnetic beam facilities with the aim of achieving a better understanding of the nucleon from QCD.

It is challenging to accurately establish the nucleon’s excitation spectrum and the properties of the individual states (e.g. photocouplings, lifetimes, spins, parities, decay branches). The resonances are broad and overlapping for all but the lowest mass states, and can interfere. To unambiguously resolve the states through partial wave analysis we require kinematically complete measurements of single- and double- polarisation observables utilising combinations of polarised photon beams, spin-polarised targets and determination of the polarisation

of the final state (recoiling) baryon [12–16]. Different states can have different photocouplings to neutron or proton targets [17, 18] and also differ in their preferred decay branches, necessitating data from a wide range of final states such as  $N\pi$ ,  $K\Sigma$ ,  $K\Lambda$ , multiple meson decays such as  $N\pi\pi$ , and even vector meson decays such as  $N\omega$  [3, 13, 19].

Nucleon calculations indicate that a number of currently “missing” or poorly established states could have escaped experimental constraint because of a stronger decay coupling to the strange sector rather than the (comparatively) well studied  $\pi N$  [3]. Recent double-polarisation measurements from proton targets in the strange-decay sector have been particularly successful in establishing new states in recent years [20–28]. Disappointingly, the current database of such reactions for neutron targets is sparse, with only a single double-polarisation measurement obtained for  $K^0\Lambda$  and  $K^0\Sigma^0$  final states[29], obtained with such large statistical uncertainties that even the sign of the observable is not well defined. In this work we present the first measurement of the double-polarisation beam-target helicity asymmetry ( $E$ ) for the reaction  $\gamma n \rightarrow K^+\Sigma^-$ , utilizing a circularly polarized tagged-photon beam and a spin polarized Hydrogen deuteride (HD) target. The measurement is an important new constraint in the current world database for  $K^+\Sigma^-$ , which currently only comprises a cross section determination with CLAS [30, 31] and a measurement of a single-polarisation observable, the beam-spin asymmetry ( $\Sigma$ ), measured in a restricted kinematics at LEPS [28].

Section (II) gives a description of the experimental setup, Section (III) introduces the polarisation observable  $E$ , and Section (IV) gives an overview of the final state selection and the analysis procedure to extract  $E$ . In section (V) the new  $E$  data is compared with current theoretical models and the implications for the neutron

---

\* nicholas@jlab.org

excited states is discussed.

## II. EXPERIMENTAL SETUP

The experiment was conducted at the Thomas Jefferson National Accelerator Facility (JLab) utilising the Continuous Electron Beam Accelerator Facility (CEBAF) and the CEBAF Large Acceptance Spectrometer (CLAS) [32] in Hall-B (see Fig. 1). CLAS is a toroidal field magnetic analysing spectrometer covering polar angles of  $\sim 8^\circ$ - $140^\circ$  with large azimuthal acceptance ( $\sim 83\%$ ) and utilising a variety of tracking, time-of-flight and calorimeter systems to provide particle identification and 4-vector determination for particles produced in electro- or photo-reactions.

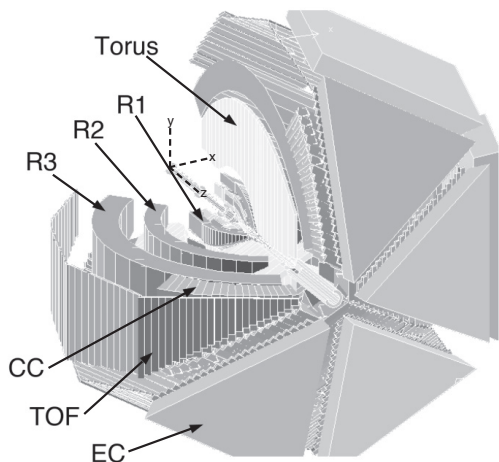


FIG. 1. A three-dimensional view of CLAS showing the torus magnet, the three regions of drift chambers (R1–R3), the Cerenkov counters (CC), the time-of-flight detector (TOF), and the electromagnetic calorimeters (EC). The CLAS reference frame, also indicated here, was defined with the  $z$  axis along the beam line and the  $y$  axis perpendicular to the horizontal. Figure taken from Ref. [32].

The current data were obtained as part of the E06-101 experiment [33] (referred to as the g14 experiment) in which an energy-tagged polarised-photon beam impinged on a 5-cm-long solid target of 23-25% polarised hydrogen deuteride [34, 35] placed in the centre of CLAS. The energy-tagged ( $\Delta E \sim 0.2\%$ ) and circularly-polarised (20-85%) photon beam was produced by impinging a longitudinally polarised electron beam on a thin copper radiator, with post-bremsstrahlung electrons momentum analysed in a magnetic tagging spectrometer [36]. During the experiment the polarisation of the photon beam was flipped pseudorandomly with  $\sim 960$  Hz flip rate between the two helicity states. The HD target polarization was also periodically flipped between directions parallel or anti-parallel to the incoming photon-beam. For more details on the experimental setup for the g14 experiment see Ref [29].

## III. POLARISATION OBSERVABLE $E$

Measurements employing a circularly-polarised photon beam in combination with a longitudinally polarised target give access to the double-polarisation observable  $E$ . The differential cross section for  $\vec{\gamma}\vec{n} \rightarrow K^+\Sigma^-$  reaction for the case of a polarised beam and target is given by [15, 37]:

$$\left(\frac{d\sigma}{d\Omega}\right) = \left(\frac{d\sigma}{d\Omega}\right)_0 (1 - P_T^{eff} P_\odot E), \quad (1)$$

where  $\left(\frac{d\sigma}{d\Omega}\right)_0$  denotes the unpolarized differential cross section,  $P_T^{eff}$  denotes the effective target polarization (accounting for events that originate from unpolarised material within the target cell), and  $P_\odot$  the degree of circular photon polarization [38]. The observable  $E$  is extracted from asymmetries,  $A$ , in the reaction yields arising from different orientations of the beam and target polarisations:

$$A(W, \cos\theta_{K^+}^{cm}) = \frac{\left(\frac{d\sigma}{d\Omega}\right)^{\uparrow\downarrow} - \left(\frac{d\sigma}{d\Omega}\right)^{\uparrow\uparrow}}{\left(\frac{d\sigma}{d\Omega}\right)^{\uparrow\downarrow} + \left(\frac{d\sigma}{d\Omega}\right)^{\uparrow\uparrow}}, \quad (2)$$

where  $\uparrow\uparrow$  and  $\uparrow\downarrow$  denote a parallel or antiparallel orientation of the photon and target polarisations respectively. The polarization observable  $E$  is then given by

$$E = \frac{1}{P_T^{eff} P_\odot} A(W, \cos\theta_{K^+}^{cm}). \quad (3)$$

This method allows the determination of  $E$  from the reaction yields for different combinations of the target-beam polarisation, while cancelling the effects of detector acceptance.

## IV. DATA ANALYSIS

Events containing a single  $K^+$  and a single  $\pi^-$  in the final state (without further restrictions on any additional neutral tracks), were selected to provide a sample of  $\gamma n(p) \rightarrow K^+\Sigma^-(p)$ , where the  $\Sigma^-$  has decayed to  $n\pi^-$  (99.8% branching ratio). Particle identification and photon selection was done following standard procedures for CLAS analyses, as summarised in Ref. [29].

The  $K^+\pi^-$  yield was further analysed to more cleanly select the reaction of interest and remove unwanted backgrounds. Due to limitations in the separation of pions and Kaons at high momenta in CLAS, a fraction of events from the  $\pi\pi$  final state were present in our yield. These were cleanly removed using simple kinematical cuts [39].

Further cuts were applied to the remaining event sample. The missing-mass of  $\gamma n \rightarrow K^+X$  as a function of  $\gamma n \rightarrow K^+\pi^-X$  was constructed, calculated assuming a stationary neutron target. Events from the reaction of interest lie where the  $MM_{\gamma n \rightarrow K^+X}$  correspond to the nominal mass of the  $\Sigma^-$  and  $MM_{\gamma n \rightarrow K^+\pi^-X}$  correspond to the

nominal mass of the neutron. Figure 2 shows the missing-mass of  $\gamma n \rightarrow K^+ X$  as a function of  $\gamma n \rightarrow K^+ \pi^- X$ . The red lines indicate the two-dimensional cuts used to select the reaction of interest. The parameters of the two-

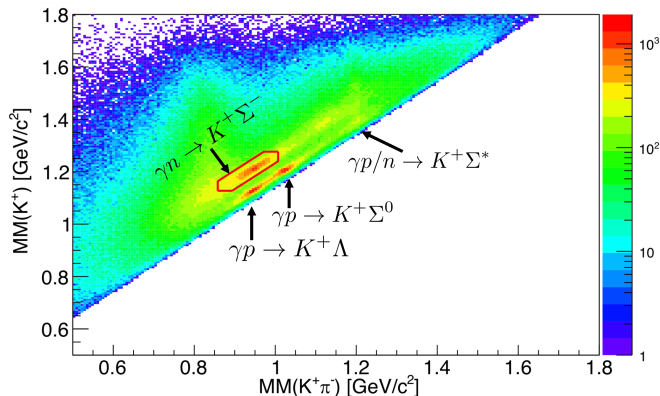


FIG. 2. Missing-mass of  $\gamma n \rightarrow K^+ X$  as a function of  $\gamma n \rightarrow K^+ \pi^- X$ . The regions where the different reaction channels contribute are indicated by the arrows on the figure. The region enclosed by the red line contains the selected events.

dimensional cut were optimised to remove background contributions while maintaining a good event sample. As indicated in Fig. 2, background channels can potentially contribute to the  $\gamma n \rightarrow K^+ \Sigma^-$  yield, mainly from  $\gamma p \rightarrow K^+ \Lambda$ ,  $\gamma p \rightarrow K^+ \Sigma^0$ , and  $\gamma p/n \rightarrow K^+ \Sigma^*$ . To quantify the contribution of background events to the event sample, the reactions were simulated, processed through the CLAS acceptance and analysed identically to the real data. The final selection cuts applied to the data were optimised to reduce the background-to-total (B2T) ratio to the level of a few percent. With the tuned cuts (Fig. 2) the dominant background of  $\gamma n \rightarrow K^+ \Sigma^{*-}$  was reduced to  $B2T_{\gamma n \rightarrow K^+ \Sigma^{*-}} < 2\%$ , while retaining around 50% of the true yield. The quantification of the background contributions allowed their effect to be included in the systematic error (see following section).

Measurements with an empty-target cell (i.e. without the HD target material) were used to quantify the contribution to the yield of events originating from the aluminium cooling wires or entrance/exit windows. These events originate from unpolarized nucleons (i.e. are associated with  $P_T = 0$ ) and account must be made for the resulting "dilution" of the effective target polarisation. This was calculated based on the ratio of empty-target to full-target data within the predetermined  $z$ -vertex cuts. This dilution factor,  $D_F$ , was then utilised in the extraction of the helicity asymmetry from the data by using the effective target polarisation:  $P_T^{eff} = D_F P_T$ .

A thorough assessment of systematic effects in the extracted ( $E$ ) observable was carried out. This included varying the applied particle identification cuts, systematics associated with the photon and target polarization, varying the vertex cuts (and therefore effective target polarisation). Further, systematic uncertainties arising

from the Fermi motion of the target nucleon were investigated and found to be small, utilising the correlation between the Fermi momentum and the missing-mass of  $\gamma n \rightarrow K^+ \Sigma^-$ . The absolute systematic uncertainties associated with the determination of  $E$  was found to be  $\Delta E^{syst} = 0.116$ . In addition, a relative systematic uncertainty that stems from the target and photon polarization as well as empty target subtraction was estimated to be  $\Delta E^{syst}/E = 6.9\%$ .

## V. RESULTS AND DISCUSSION

The measured beam-target polarisation observable  $E$  is presented in fig. 3 for six centre-of-mass energy ( $W$ ) bins between 1.7 and 2.3  $\text{GeV}/c^2$  and for six bins in  $K^+$  center-of-mass angle ( $\theta_{K^+}^{cm}$ ) [40]. The angular bins have varying widths reflecting the angular variation in the reaction yield. The experimental data show a positive value of  $E$  for most of the sampled bins. As  $E$  must have a value of  $+1$  at  $\cos \theta_{K^+}^{cm} \rightarrow \pm 1$  to conserve angular momentum, values of  $E$  outside of our measured region must vary rapidly. The lines in Fig. 3 are the predictions of the  $E$  observable from the Kaon-MAID-2000 (green), Kaon-Maid-2017 (magenta) and Bonn-Gatchina-2017 (black) PWA models. It is clear that the models give rather divergent predictions for this observable, and none of the current solutions give consistent agreement with the experimental data over the sampled kinematic range. This suggests that the relevant photoproduction amplitudes are not well constrained by the current world-data, and that the new data has the potential to provide new information. The current Bonn-Gatchina-2017 solution is fitted the entire database of meson photoproduction from the nucleon. In this solution the only direct  $K^+ \Sigma^-$  constraints in the database are from the cross section determination [30, 31] [41].

In Fig. 4 the impact of including the new data in the Bonn-Gatchina database are explored. The predictions of  $E$  from this new fit (Bonn-Gatchina-2019) are shown by the red line [42]. It is seen that the new solution gives a much improved fit to the data. (for comparison Bonn-Gatchina-2017 solution is repeated on this figure (black line)). The implications of the new Bonn-Gatchina-2019 for properties of the excited states are shown in Table I, where the helicity couplings calculated at the pole position are compared with previously published values [44]. The new solution has a different interference between the  $S_{11}$  and  $P_{13}$  partial waves than indicated in earlier fits, now better constrained by data as the  $E$  observable allows separation of the helicity projections  $1/2$  and  $3/2$  (corresponding to projections of the  $S_{11}$  and  $P_{13}$  respectively). As a result the new data produces significant changes in the extracted photocouplings of the individual states, particularly the  $N(1720)$  and  $N(1900)$  as indicated in Table I. The helicity  $1/2$  coupling of the  $P_{13}(1720)$  state has the same value as before but is rotated in phase by 90 degrees, while the corresponding helicity coupling

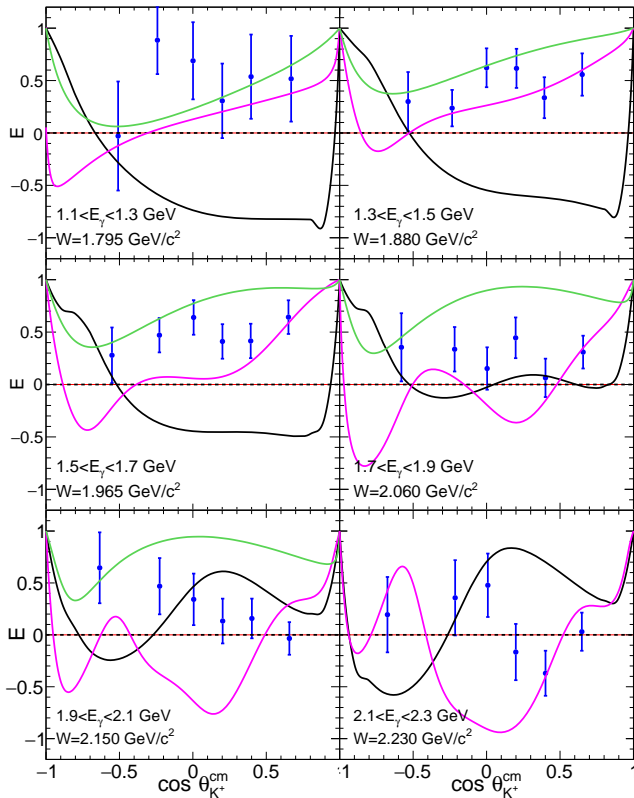


FIG. 3. Angular dependence of the determined beam-target double polarisation observable  $E$  (with combined statistical and systematic uncertainties) for the six center-of-mass energy  $W$  bins compared with the Kaon MAID 2000 (green) and 2017 (magenta), as well as predictions from Bonn-Gatchina (black). The event-weighted  $W$  value and the photon-energy bin are indicated in the panels.

of the  $P_{13}(1900)$  state has decreased by almost factor 2. This results in a different behavior of the  $P_{13}$  1/2 helicity amplitude whose interference with the  $S_{11}$  partial wave defines the behavior of the  $E$  observable. The 3/2 helicity coupling of  $P_{13}(1720)$  notably decreases and is rotated by 85 degrees while the 3/2 helicity coupling of the  $P_{13}(1900)$  state did not exhibit significant changes.

As a further check, the agreement of the Bonn-Gatchina-2019 solution with the existing cross section data was also studied (red line in left panels of Fig. 5). A rise in the  $K\Sigma$  cross section at backward kaon angles is now suggested, which is generally consistent with the sparse data in this region. The improved agreement of the new solution with the existing beam asymmetry data from LEPS [28] for  $K\Sigma$  is also presented in Fig. 5.

The sensitivity of the new  $E$  data to missing or poorly established excited states was also explored within the Bonn-Gatchina framework. The database for reactions off neutron targets is much smaller than for the proton, so there is the potential to gain new sensitivities with the current data. There is significant current interest to gain sensitivity to the  $D_{13}(2120)$ , being a resonance

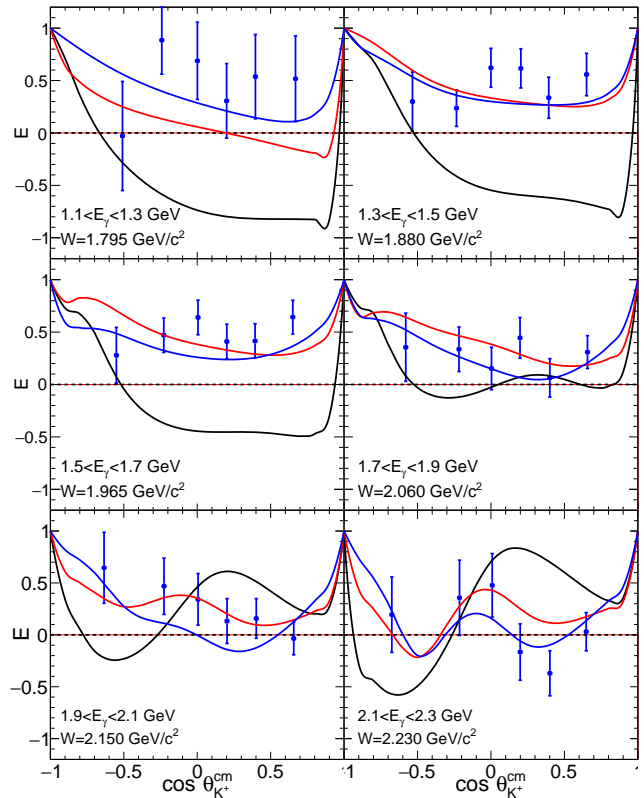


FIG. 4. The new Bonn-Gatchina description of the helicity asymmetry data. The published solution [43] is shown with the full black curves. The solutions with the new data on the helicity asymmetry included in the fit is shown with the red full lines. The solution with added  $D_{13}$  state is shown with the blue full lines.

TABLE I. The  $\gamma N$  helicity couplings of nucleon states ( $GeV^{-1/2}10^{-3}$ ) calculated as residues in the pole position. The first lines (for every state) show the numbers published earlier [44] and the present values are shown with the second lines. Only resonances which either are most important for the description of the new data or are deviated by more than one standard deviation from the published results are included.

	$A_{1/2}$	Phase	$A_{3/2}$	Phase
$N(1895)1/2^-$	$-15 \pm 10$	$60 \pm 25^\circ$		
$N(1895)1/2^-$	$-20 \pm 7$	$50 \pm 20^\circ$		
$N(1720)3/2^+$	$-25^{+40}_{-15}$	$-75 \pm 35^\circ$	$100 \pm 35$	$-80 \pm 35^\circ$
$N(1720)3/2^+$	$-45 \pm 15$	$20 \pm 30^\circ$	$-35 \pm 20$	$-15 \pm 30^\circ$
$N(1900)3/2^+$	$-98 \pm 20$	$-13 \pm 20^\circ$	$74 \pm 15$	$5 \pm 15^\circ$
$N(1900)3/2^+$	$-45 \pm 15$	$-5 \pm 20^\circ$	$80 \pm 12$	$0 \pm 20^\circ$

predicted by many theoretical models of nucleon structure but not escaping proper experimental confirmation. The Bonn-Gatchina fits were repeated with the addition of additional states, one at a time, with varying properties. The best description of the new data was obtained when adding a  $D_{13}$  resonance of mass 2170 MeV. The results of this new fit (Bonn-Gatchina-2019-2) are shown

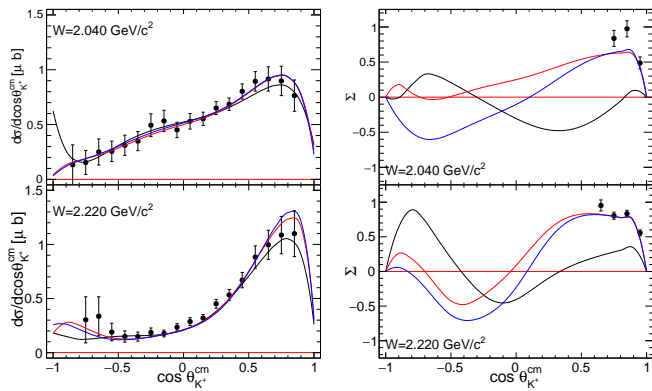


FIG. 5. The description of the differential cross section (data from [30]) (left) and the beam asymmetry (data from [28]) (right). The published solution [43] is shown with the full black curves. The solutions with the including new data on the helicity asymmetry is shown with the red full lines. The solution with added  $D_{13}$  state is shown with the blue full lines.

by the blue lines in Figs 4 and 5. The new  $E$  data are consistent with such a  $D_{13}$  contribution, which results in improved fits for many of the sampled  $W$  and  $K^+$   $c.m.$  angle ranges. However, the level of improvement in the description of the  $E$  observable is not sufficient to make strong claims. The new solution does however provide a basis to explore sensitivities in other observables. The  $D_{13}$  has a strong predicted influence on the beam asymmetry and future measurement over a wider angular range could provide valuable constraints on its existence (e.g. see Fig. 5). Other possibilities were also explored. The inclusion of a missing ( $D_{15}$ ) also improved the agreement with data, while no improvement was obtained by including missing states with positive parity.

## VI. SUMMARY

We present the first measurement of a double-polarisation beam-target observable ( $E$ ) for the reaction  $\gamma n \rightarrow K^+\Sigma^-$ , utilizing a circularly polarized photon beam and a spin polarized HD target. The new  $E$  data is an important addition to the sparse world database constraining the strange decays of excited neutron states. Model predictions for the  $E$  observable in this channel were strongly divergent and none gave a good description of the new data over the full kinematic range. Fitting the new data in the framework of one of the models (Bonn-Gatchina) resulted in new constraints in the interference of the  $S_{11}$  and  $P_{13}$  partial waves, and significant changes in the extracted photocoupling of a number of resonance states, including the  $N(1720)$ ,  $N(1895)$ , and  $N(1900)$ . Improved fits to the new  $E$  data could be obtained with the inclusion of a "missing"  $D_{13}(2120)$  resonance, although further measurements are clearly necessary to better establish this state.

## VII. ACKNOWLEDGMENTS

This work has been supported by the U.K. STFC (ST/P004385/1, ST/P004008/1, and ST/L00478X/1) grants. We also acknowledge the outstanding efforts of the staff of the Accelerator and Physics Divisions at Jefferson Lab that made this experiment possible. The Southeastern Universities Research Association (SURA) operated the Thomas Jefferson National Accelerator Facility for the United States Department of Energy under contract DE-AC05-06OR23177. Further support was provided by the National Science Foundation, the United Kingdom's Science and Technology Facilities Council, the Italian Istituto Nazionale di Fisica Nucleare, and the National Research Foundation of Korea.

- 
- [1] I. G. Aznauryan *et al.*, Int. J. Mod. Phys. E **22** (2013).
  - [2] S. Capstick and W. Roberts, Prog. Part. Nucl. Phys. **45** (2000).
  - [3] S. Capstick and W. Roberts, Phys. Rev. D **58** (1998).
  - [4] S. Capstick and N. Isgur, Phys. Rev. D **34** (1986).
  - [5] U. Loring, B. C. Metsch, and H. R. Petry, Eur. Phys. J. A **10** (2001).
  - [6] L. Y. Glozman, W. Plessas, K. Varga, and R. F. Wagenbrunn, Phys. Rev. D **58** (1998).
  - [7] M. M. Giannini, E. Santopinto, and A. Vassallo, Eur. Phys. J. A **12** (2001).
  - [8] R. G. Edwards, J. J. Dudek, D. G. Richards, and S. J. Wallace, Phys. Rev. D **84** (2011).
  - [9] J. Dudek and R. Edwards, Phys. Rev. D **85** (2012).
  - [10] R. G. Edwards, N. Mathur, D. G. Richards, and S. J. Wallace, Phys. Rev. D **87** (2013).
  - [11] S. J. Brodsky, Eur. Phys. J. A **31** (2007).
  - [12] C. G. Fasano, F. Tabakin, and B. Saghai, Phys. Rev. C **46** (1992).
  - [13] W.-T. Chiang and F. Tabakin, Phys. Rev. C **55** (1997).
  - [14] G. Keaton and R. Workman, Phys. Rev. C **54** (1996).
  - [15] A. M. Sandorfi, S. Hoblit, H. Kamano, and T. S. H. Lee, J. Phys. G **38** (2011).
  - [16] J. Nys, J. Ryckebusch, D. G. Ireland, and D. I. Glazier, Phys. Lett. B **759** (2016).
  - [17] A. M. Sandorfi and S. Hoblit, Nucl. Phys. A **914** (2013).
  - [18] T. Mart, C. Bennhold, and C. E. Hyde-Wright, Phys. Rev. C **51** (1995).
  - [19] S. Capstick and W. Roberts, Phys. Rev. D **57** (1998).
  - [20] K. H. Glander *et al.*, Eur. Phys. J. A **19** (2004).
  - [21] R. Castelijns *et al.*, Eur. Phys. J. A **35** (2008).
  - [22] M. Nanova *et al.*, Eur. Phys. J. A **35** (2008).
  - [23] R. Bradford *et al.*, Phys. Rev. C **73** (2006).
  - [24] M. E. McCracken *et al.*, Phys. Rev. C **81** (2010).
  - [25] M. Sumihama *et al.*, Phys. Rev. C **73** (2006).
  - [26] J. W. C. McNabb *et al.*, Phys. Rev. C **69** (2004).
  - [27] A. Lleres *et al.*, Eur. Phys. J. A **31** (2007).
  - [28] H. Kohriet *et al.*, Phys. Rev. Lett. **97** (2006).
  - [29] D. Ho *et al.*, Phys. Rev. C **98** (2018).
  - [30] S. A. P. *et al.*, Phys. Lett. B **688** (2010).

- [31] N. Compton *et al.*, Phys. Rev. C **96** (2017).
- [32] C. D. Bass *et al.*, Nucl. Instrum. Meth. A **503** (2003).
- [33] F. Klein *et al.*, CLAS Approved Experiment **E06-101**.
- [34] M. Lowry *et al.*, Nucl. Instr. Meth. A **815** (2016).
- [35] C. D. Bass *et al.*, Nucl. Instrum. Meth. A **737** (2014).
- [36] D. I. Sober *et al.*, Nucl. Instrum. Meth. A **440** (2000).
- [37] I. S. Barker, A. Donnachie, and J. K. Storrow, Nucl. Phys. B **95** (1975).
- [38] The photon polarisation was determined using the Maximon and Olsen formula (H. Olsen and L. C. Maximon, Phys. Rev. 114, 887 (1959)) utilising the energy of the incident and bremsstrahlung electrons, as well as the polarisation of the incident electron beam, which was periodically measured using the Moller polarimeter (J. M. Grames *et al.*, Phys. Rev. ST Accel. Beams 7, 042802 (2004)).
- [39] For correctly identified events the missing mass of  $\gamma n \rightarrow K^+ \pi^- X_1$  reconstructs the neutron mass from the  $\Sigma^-$  decay. To aid the identification of the background events, the missing mass of  $\gamma n \rightarrow \pi^+ \pi^- X_2$  was also calculated for each event, assuming the pion mass for the “Kaon”.
- [40] The centre-of-mass frame is calculated assuming the target neutron at rest. However, the effect of Fermi motion on the value of  $W$  is small compared to the bin widths. The reported  $W$  value for each  $E_\gamma$  bin (see figure) is obtained from the event-weighted mean of the  $E_\gamma$  distribution.
- [41] Two solutions are presented in the reference. In Fig \*\* we present the one which gave the best fit to the new data.
- [42] Note that the new fit also included the beam asymmetry data in very forward Kaon kinematics from LEPS which was not included in the previous Bonn-Gatchina-2017 fit.
- [43] A. V. Anisovich *et al.*, Phys. Lett. B **772** (2017).
- [44] A. V. Anisovich *et al.*, Phys. LRev. C **96** (2017).